

Changes on structural characteristics of cellulose pulp fiber incubated for different times in anaerobic digestate

Gustavo Henrique Denzin Tonoli^{1ID}, Kevin Holtman¹, Luiz Eduardo Silva^{1ID*}, Delilah Wood^{2ID},
Lennard Torres^{2ID}, Tina Williams^{2ID}, Juliano Elvis Oliveira^{2ID}, Alessandra Souza Fonseca¹,
Artur Klamczynski¹, Gregory Glenn^{2ID}, William Orts^{2ID}

¹Federal University of Lavras, Lavras, Minas Gerais, Brazil

²USDA-ARS, Western Regional Research Center, Bioproducts Research Unit, 800 Buchanan Street, Albany, CA 94710

TECHNOLOGY OF FOREST PRODUCTS

ABSTRACT

Background: The objective of the present work was to investigate the influence of a pre-treatment of microbial-rich digestate (liquid mesophilic anaerobic digestate – AD-supernatant) on the morphology, crystallinity, and thermal stability of cellulose pulp fiber.

Results: The six most abundant bacteria in the AD-supernatant were determined by 16S analysis. The bacteria population was comprised mostly of *Bacteroides graminisolvens* (66%) and *Parabacteroides chartae* (28%). Enzymatic activity from the bacteria partially removed the amorphous components and increased the crystallinity and crystallite size of the cellulose substrate. The fiber pulp was incubated in AD-supernatant for 5, 10, and 20 days. The X-ray diffraction data provided evidence that the amorphous portion of the cellulose was more readily and quickly hydrolyzed than the crystalline portion. The longest incubation times (20 days) resulted in substantial deconstruction of the cellulose fiber structure and decreased the thermal degradation temperature.

Conclusion: The anaerobic digestate is inexpensive and could be used to effectively aid in the pre-treatment of cellulose on large scale transformation processes, e.g. for making biofuels, cellulose micro/nanofiber production or engineered fiber-based materials.

Keywords: Crystallinity; lignocellulosic fibers; enzymatic digestion; hydrolysis

HIGHLIGHTS

Selective enzymatic hydrolysis resulted in higher crystalline content.
AD-supernatant is affective and milder than acid hydrolysis.
Higher water accessibility occurred when samples are less crystalline.
Treatments with AD-supernatant may be useful for partially degrading pulp fiber.

TONOLI, G. H. D. ; HOLTMAN, K.; SILVA, L. E.; WOOD, D.; TORRES, L.; WILLIAMS, T.; OLIVEIRA, J. E.; FONSECA, A. S.; KLAMCZYNSKI, A.; GLENN, G.; ORTS, W. Changes on structural characteristics of cellulose pulp fiber incubated for different times in anaerobic digestate. CERNE, v. 27, e-102647, doi: 10.1590/01047760202127012647

*Corresponding author

e-mail: lesilvaflorestal@gmail.com

Received: 03/07/2020

Accepted: 06/01/2021



INTRODUCTION

A two-component cellulose model has been used to describe cellulose chains as containing both crystalline (ordered) and amorphous (less ordered) domains (French, 2014). The relative degree of crystallinity and recalcitrance of cellulosic materials is of great importance because of its bearing on their deconstruction for biorefinery purposes or application and functional performance of plant fibers (Yang *et al.*, 2011).

Microbes which secrete extracellular enzymes have the potential to be a powerful tool for modifying the properties of cellulose and decrease recalcitrance by various degradation reactions (Cao and Tan, 2005). The enzymatic modification of cellulose may help improve fiber processing technologies including pulping and pulp bleaching (Moreira *et al.*, 2015). It could also improve fiber deconstruction and generation of micro/nanofibrils (Tonoli *et al.*, 2016, Durães *et al.*, 2020) that can be used for specific applications such as in fiber-reinforced composites (Fonseca *et al.*, 2016), films (Silva *et al.*, 2020; Silva *et al.*, 2019), and paper (Viana *et al.*, 2018) or as a feedstock for biofuels (Yang *et al.*, 2011). Durães *et al.* (2020) reported the effects of commercial enzymes on the fiber cell wall morphology and on increasing the fiber dislocations (kinks), but no information about crystallinity was reported. Reports indicate that the amorphous portion of cellulose is degraded more easily by enzymes than the less accessible crystalline regions (Cao and Tan, 2005; Cao and Tan, 2004). As a result, the overall crystalline content of a cellulose substrate increases (until a certain level) with enzyme treatment and, consequently, the cellulose substrate becomes more resistant to further hydrolysis (Imai *et al.*, 2020).

The degree of crystallinity of cellulose is commonly controlled/manipulated by treating the cellulose with concentrated acids or alkalis for a controlled period of time and temperature (Prado *et al.*, 2018). These treatment conditions facilitate swelling and hydrolysis of the amorphous portions of the cellulose at the desired rates. In most cases, acid and alkali treatments of cellulose generate large quantities of waste that must be recovered and properly discarded at a considerable effort and expense (Wyman *et al.*, 2004). Enzymatic treatment has attracted considerable interest as an environmentally sound process that uses milder hydrolysis conditions as compared with acid hydrolysis. Furthermore, enzymatic hydrolysis does not involve the use of solvents or harsh chemical reagents that must be recovered and disposed of at a considerable expense (Meyabadi and Dadashian, 2012). Studies on the potential use and action of cellulases or purified cellulases have revealed the mechanism and kinetics involved in enzymatic cellulose degradation (Rabinovich *et al.*, 2002).

Very few studies have been reported using anaerobic bacteria as compared to aerobic bacteria (and also with fungi) to modify cellulose structure, especially crystallinity. The novelty in the present work is the use of liquid anaerobic digestate as a treatment for etching away amorphous regions of Eucalyptus Kraft pulp fibers, and further investigation is merited. Bleached eucalyptus

pulp fibers were exposed here to an anaerobic microbial-rich digestate for different incubation periods (5, 10 and 20 days) to resolve the treatment effect on morphology, crystallinity, and thermal stability of the fibers.

MATERIAL AND METHODS

Materials

Eucalyptus (hybrid: *Eucalyptus urophylla* × *Eucalyptus grandis*) bleached Kraft pulp was used as starting raw-material. The cellulose portion was composed of ~92.2 wt.% β -cellulose, 6.9 wt.% α -cellulose and 0.9 wt.% γ -cellulose, according to TAPPI T 203 cm-99 (TAPPI, 2009) standard. Its hemicelluloses (SCAN, 1961) and lignin (SCAN, 1977) contents were 13.9 wt.% and 0.1 wt.%, respectively; while extractives (SCAN, 1962) and ash (SCAN, 1962) contents were around 0.1 wt.% and 0.6 wt.%, respectively.

Digestate treatment of the fibers in the AD-supernatant

The anaerobic digestion system was comprised of a 5 L four-neck flask set with a submerged withdrawal tube, 2 return lines, and a gas outlet. Mesophilic liquid anaerobic digestate (AD-supernatant) was obtained from the medium solids (20% solids) anaerobic reactor feed with substrate of paper pulp obtained from steam autoclaving of municipal solid waste (MSW). The reactor flask was designed so that the bacterial population was contained in an attached growth media, in such a way that only liquid permeate was withdrawn and recirculated. It was from this recirculation line that the AD-supernatant, containing the extracellular enzymes, was taken. (Fig.1). The AD-supernatant genetic sequence and characterization was performed as reported in Tonoli *et al.* (2016).

Cellulose pulp fibers (with around 6% moisture) were finely milled in a Wiley mill to pass a 0.5 mm mesh screen in order to obtain fiber particles with their extremities more reactive to treatment. The milled pulp (control) in a concentration of about 0.06 g of pulp per mL of AD-supernatant was then put in direct contact with the AD-supernatant and maintained in a closed system at 37°C for up to 20 days. Samples were taken after 5, 10 and 20 days and centrifuged in order to separate the solubilized substances from the material to be analyzed. The mass loss during the digestate treatment was estimated using samples dispensed into 20 kD dialysis tubes, incubated for the same period, and the difference in mass was calculated between the initial and final residual amounts.

Fiber characterization

Fiber morphology

A Leica DM4000B compound light microscope (LM) was used to investigate the morphology of milled (control) and treated fibers. Suspensions were previously stained with a drop of ethanol-safranin solution (0.5% v/v) to increase

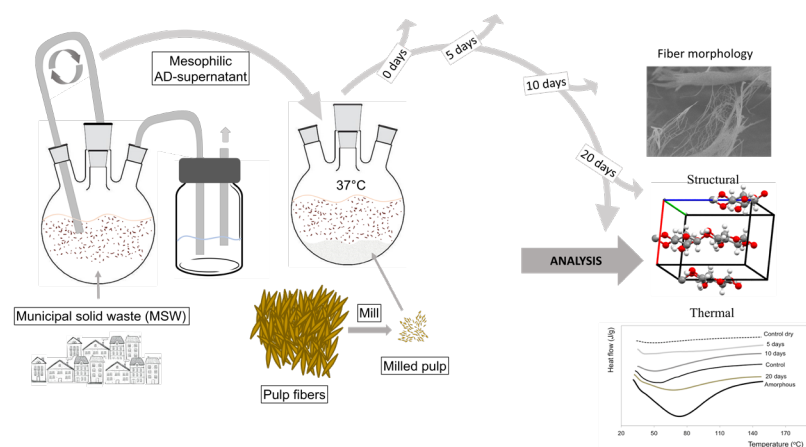


Fig. 1 Illustrative flow chart of the digestate treatment. After treated with the AD-supernatant, the samples were collected from the recirculation line at 0, 5, 10 and 20 days.

contrast between phases. The birefringence of treated fibers was monitored by polarized light and micrographs were acquired from typical samples as reported in Durães *et al.* (2020).

Fiber samples before and after treatment were freeze-dried for analyses in a Hitachi S-4700 field emission scanning electron microscope (FESEM). The samples were mounted on a specimen stub using double adhesive coated carbon tabs (Ted Pella). The samples were coated with gold-palladium in a Denton Desk II sputter coating unit (Denton Vacuum). Finally, the samples were viewed in the FESEM.

X-ray diffraction (XRD) and true density of the fibers

X-ray diffraction (XRD) patterns were acquired for milled and treated fibers with an X-ray diffractometer (Philips DY971), using $\text{CuK}\alpha$ radiation at 45kV and 40mA. Scattered radiation was detected in the range of $2\theta = 5\text{--}40^\circ$, at a scan rate of $2^\circ/\text{min}$. Crystalline fraction (CF) was determined as reported by French (French, 2014) and Correia *et al.* (2016) (Eq. 1).

$$\text{CF} = \frac{A_e - A_a}{A_e} \cdot 100 \quad [1]$$

Where A_e and A_a are the areas under the experimental powder pattern and the amorphous theoretical curve, respectively. Therefore, to determine the CF, the Mercury 3.7 program (French 2014; Macrae *et al.*, 2008) was used to produce theoretical diffraction curves, varying FWHM of cellulose I β , which is the most abundant cellulose polymorph occurring in nature for higher plants (Nam *et al.*, 2016). For amorphous halo it was used cellulose II with FWHM=9 and a correction factor to fit under the experimental curves Correia *et al.* (2016). After the fitting process, all measurements for crystallite size and number of cellulose chains were carried out on the theoretical curves. The CIF (Crystallographic Information File) were obtained from complementary data (French, 2014) and edited for each different fiber on CIF files to fit the theoretical curve into the experimental one, as reported elsewhere (Fonseca *et al.*, 2019; French 2014). All intensities were normalized to

optimize the fitting of the patterns. In order to help explain crystalline results, Segal's crystalline index (CI) (Segal *et al.*, 1959) was also calculated. CI was estimated from the heights of the (200) peak ($2\theta \sim 22.5^\circ$) and the minimum intensity between the (110) and (200) peaks (2θ between 16° and 22°) that is related to the amorphous fraction (French, 2014). Segal's CI it is an easy and fast way of assessing crystalline data. Although, it is not an accurate method, and researchers have been encouraged to move on to simulation analysis and fitting methods (French, 2020), such as Theoretical analysis with Mercury software (Nam *et al.*, 2016; French *et al.*, 2014).

Crystallite size (CS) was estimated through use of the Scherrer Eq. (2) (Cao and Tan, 2005), where CS is the size (nm) perpendicular to the lattice plane represented by the peak related to the (200) plane; K is a constant related to the crystal shape ($K=0.89$); λ is the wave length of the incident X-ray (1.54056 \AA); θ is the Bragg angle corresponding to the (200) plane (i.e. half of the 2θ value in the position of the peak); and β the peak FWHM (in radians) of the (200) reflection.

$$\text{CS} = \frac{K\lambda}{\beta \cos\theta} \quad [2]$$

True density of the fibers was also determined in order to monitor the influence of the exposure to AD-supernatant on the fiber structure. Around ten values of true density for each treatment were measured using a gas (Helium) pycnometer (AccuPyc II 1340 Series Pycnometer, Micromeritics Instrument Co.).

Differential scanning calorimetry (DSC)

Since differential scanning calorimetry (DSC) measures energy flow from a sample to a reference, it is possible to use this technique to measure the energy changes produced during cellulose dehydration (Bertran and Dale, 1986). In a typical DSC curve of cellulose fibers, an endothermic peak occurs between 30 and 150°C (Chan *et al.*, 2013). The area of this endothermic peak can be measured and it is proportional to the heat of dehydration required to desorb water from cellulose and evaporate (dehydration). Considering that crystalline domains of cellulose only absorb

a very small amount of moisture, water sorption in cellulose happens almost entirely in the amorphous regions (Bertran and Dale, 1986). Then, since accessibility to water (cellulose moisture content) is directly proportional to the amorphous content of cellulose, the amount of energy required to dehydrate the cellulose sample can be taken as a direct measure of its amorphous portion, and by difference it is possible to estimate the crystalline portion (Chan et al., 2013).

A TA Instruments (New Castle, DE) differential scanning calorimeter (DSC) 2910 was used to measure the heat of dehydration and estimate the degree of crystallinity (DC) of the fibers. The amorphous sample obtained by ball milling (the same for XRD amorphous pattern) was used as standard amorphous cellulose. All samples were conditioned at room temperature (~25°C) in a 60% relative humidity chamber containing KI and NH₄NO₃ saturated solutions for at least 240 h prior to each test. Around 8 mg of each sample and two repetitions were used in standard (not sealed) DSC pans and heated at a rate of 10°C/min, from 30°C to 200°C. The sample chamber was purged with nitrogen gas at a flow rate of 60 L.min⁻¹. The heat of dehydration was estimated by using the TA Instruments Universal Analysis 2000 software that integrates the peak areas and calculates the corresponding energy changes between specified temperatures. Degree of crystallinity (DC) by DSC was determined according to Bertran & Dale (1986), as the ratio between the heat of dehydration of a preconditioned sample at constant relative humidity and the dehydration heat of the completely amorphous cellulose, preconditioned under the same conditions.

Thermogravimetry

Fibers were evaluated by thermogravimetric analysis (TGA) in a Perkin Elmer Pyris 1 TGA instrument. Dried samples (~6 mg dry basis) were heated in a Pt crucible from 25 to 500°C in air flowing at 60 mL.min⁻¹ and heating rate of 10°C.min⁻¹. Critical weight loss temperatures (Tonset) were obtained from the onset points of the TGA curves, which are represented by the intersection of the extrapolated line extended from the beginning of the thermal event, with the tangent of the curve in the thermal event (Tonoli et al., 2012).

RESULTS AND DISCUSSION

Microbial identification in the mesophilic AD-supernatant

Tab.1 depicts the six most numerous bacterial species found in the mesophilic AD-supernatant. Bacterial species may have been isolated from several dilutions of both 5% sheep's blood and anaerobic phenylethyl alcohol agar, but only the plate and dilution that provided the highest quantity is listed here. All species listed below belong to Bacteroidetes and Firmicutes bacteria phyla, which are commonly found in feces of different mammals, including humans (Li et al., 2020). Among the bacterial species identified in the AD-supernatant solution, the most representative were *Bacteroides graminisolvens* and *Parabacteroides chartae* constituting more than 94% of the

total bacteria population. The hydrolytic enzyme activity on vegetable cellulose (e.g. cellulases) and hemicelluloses (e.g. xylanases) of *B. graminisolvens* are noted for their role in the biomass degradation (Chassard et al., 2010), while *Parabacteroides* species are mainly saccharolytic, producing acetic acid and succinic acid as the major end-products of fermentation (Tan et al., 2012).

Belonging to Firmicute phylum, the *Clostridium* genus usually lives in anaerobic environments such as in aquatic sediments, in the intestinal tract of humans and animals, and water-logged soils (Leja et al., 2011). They produce powerful extracellular enzymes (e.g., dehydrogenases and cellulases) that also degrade lignocellulosic materials (Wirth et al., 2012).

Morphological characteristics of the fibers

Fig. 2 shows images of the cellulose pulp fibers after they were milled. This grinding process decreased the average length of the fibers significantly (from ~0.7 mm to ~0.3 mm). However, swelling capacity is increased, by more available surface area due to fracture of part of the fibrils. Grinding is expected to increase enzyme access to fiber components and facilitate enzyme degradation (Tonoli et al., 2016).

Micro-organisms in the AD-supernatant secrete several enzymes including cellulases and hemicellulases which act synergistically in the hydrolysis of cellulose fibers as opposed to the degradation of fibers via the action of a single specific enzyme (Siqueira et al., 2010; Siro and Plackett, 2010). Light microscopy images show that cellulose fibers fragment with hydrolysis of the fiber wall from enzymatic activity when exposed for 5 to 20 days in liquid anaerobic digestate (arrow 1 in Fig 2). Swelling, caused by the enzymes, helps deconstruct the fiber cell wall, increasing fibrillation (arrows 3 in Fig 2), when compared to an intact fiber (arrows 2 in Fig 2). Severe swelling of the fiber can be referred as ballooning, due to the similarity of an expanded balloon (Tonoli et al., 2016; Le Moigne and Navard, 2010), and eventually bursts causing characteristic cell wall disruption (arrows 3 in Fig 2). Even though light microscopy does not have the range to visualize particles less than 1 μm, micro/nanofibrils still interact with light, leaving a blurred aspect near the deconstructed fiber.

Before incubation in the AD-supernatant, the fiber was birefringent (arrow 4 in Fig. 2d) because cellulose chains were uniaxially oriented. This property of birefringence is usually used to measure the angle of orientation of the microfibrils in an individual fiber (Lima et al., 2014). Arrows 4 in Fig. 2g, 2k and 2p show that birefringence decreased in various regions of the fiber after the enzyme hydrolysis, where micro/nanofibrils appeared detached from the fiber cell wall. The results validate the hypothesis that incubation of kraft pulp fiber in AD-supernatant may be an effective way to obtain micro-fragments from which nanofibers can be more readily extracted. AD-supernatant bacteria produce a myriad of enzymes like exoglucanase, able to specifically attack cellulose at its reducing end, and endoglucanase that can randomly attack its amorphous regions along the fiber (Campos et al. 2013). Thus, this pretreatment needs to be performed with precaution, considering the incubation

Tab. 1 Top six bacterial species and colony forming units (CFU) isolated from the AD-supernatant.

Phyla	Bacterial species	Characteristics	CFU ¹ / mL	Quantity
Bacteroidetes	<i>Bacteroides graminisolvens</i>	Gram-negative; non-spore-forming	78x10 ⁶	66%
	<i>Parabacteroides chartae</i>		33x10 ⁶	28%
	<i>Parabacteroides distasonis</i>		2x10 ⁶	<2%
Firmicutes	<i>Clostridium sartagoforme</i>	Gram-positive; endospore forming	3x10 ⁶	<3%
	<i>Clostridium bifermentans</i>		1x10 ⁶	<1%
	<i>Clostridium butyricum</i>		1x10 ⁶	<1%

¹ CFU is a rough estimate of the number of viable bacteria cells in a sample.

time, since the enzymes present in AD-supernatant will continue degrading and peeling away the glucose units from cellulose fibrils, thereby decreasing nanofiber dimensions and DP (Imai *et al.*, 2020). This statement is confirmed by the estimate of mass loss during the digestate treatment, whose incubation for 5, 10 and 20 days led to mass loss of around 13%, 26% and 55%, respectively, that could directly be correlated with a decrease in DP and therefore, length of the fibers.

Another benefit of AD-supernatant treatments is that they may quickly degrade non-crystalline cellulosic or other fiber components. For example, vessels (arrow 5 in Fig. 2) were not observed in the samples exposed to AD-supernatant. This is likely because vessels are comprised of less crystalline cellulose that can be readily hydrolyzed by enzymes in the AD-supernatant.

The drastic changes in the surface morphology of the eucalyptus pulp fibers before and after incubation in AD-supernatant were observed by using FESEM (Fig. 3). The control fibers had a relatively flat, smooth surface (Fig. 3a-b), while pretreated fibers had a fibrillated structure formed by micro/nanofibrils (Fig. 3c-h), showing the disruption of the fiber structure by enzymatic hydrolysis.

Crystallinity changes by XRD measurements

Fig. 4 depicts the cellulose chains disposition in the unit cell, X-ray diffractograms (XRD), and theoretical analysis of the samples. The XRD patterns of the fibers present an amorphous broad hump and crystalline peaks that are typical of semi-crystalline materials. All fiber samples exhibited a sharp peak at $2\theta = 22.6^\circ$, which is assigned to the (200) lattice plane of cellulose I.

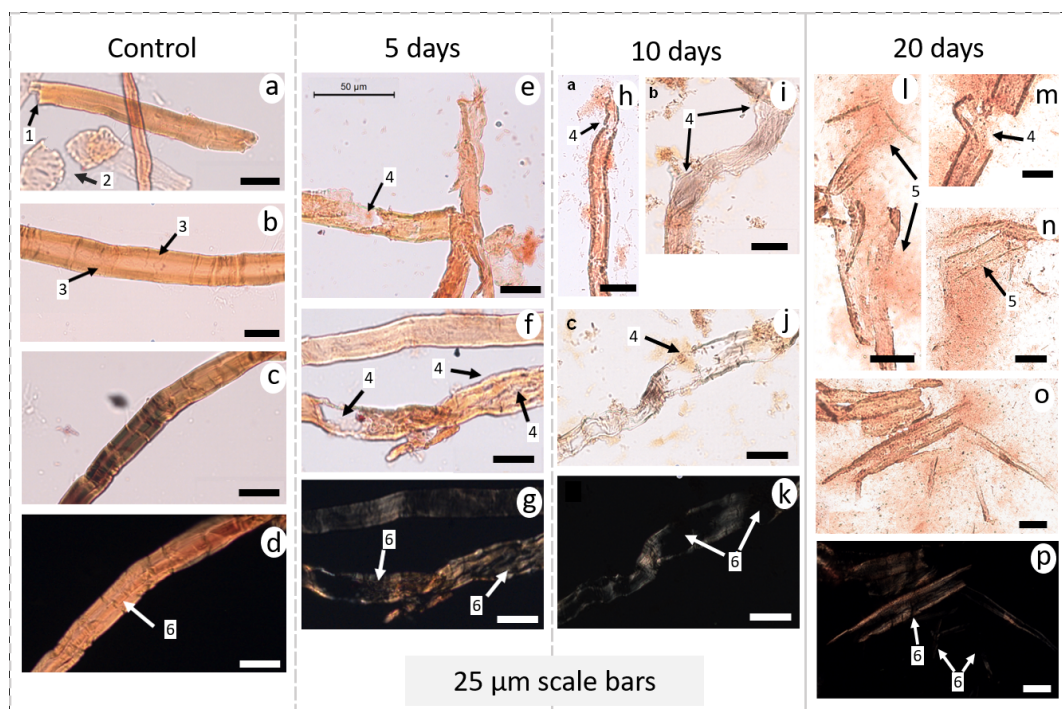


Fig. 2 Typical light microscopy (LM) images of cellulose fibers after grinding and enzymatic treatments. A-d) milled cellulose fibers; e-g) cellulose fibers after incubation for 5 days; h-k) cellulose fibers after incubation for 10 days; l-p) cellulose fibers after incubation for 20 days; d, g, k, p) transmitted light with crossed polarizers of the same region as the previous image. Arrows: 1) shows broken extremities of the fibers after grinding; 2) wood vessels; 3) Intact cell wall; 4) fiber swelling and disruption, caused by enzymatic activity; 5) fiber fibrillation into micro/nanofibrils; and 6) birefringence loss of the fiber with each treatment.

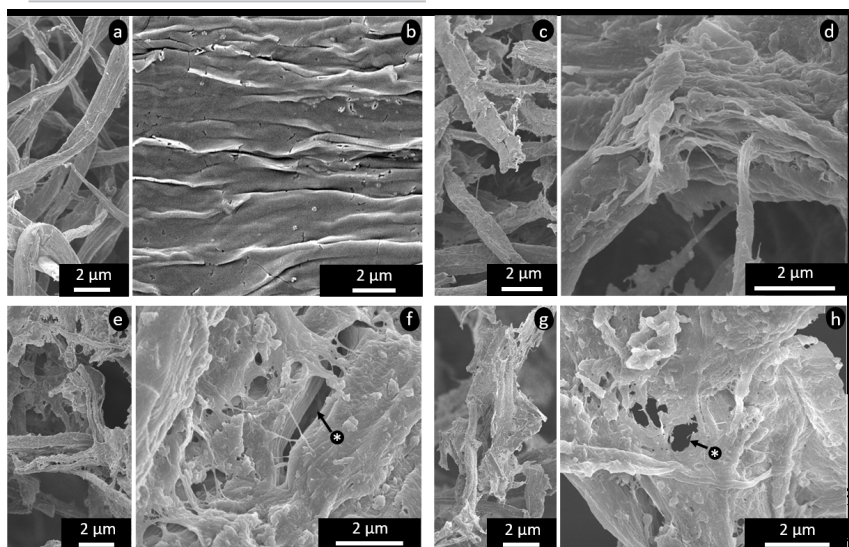


Fig. 3 Typical field emission scanning electron microscopy – FESEM images, composed of general view and fiber surface. A-b) milled cellulose fibers; c-d) cellulose fibers after incubation for 5 days; e-f) cellulose fibers after incubation for 10 days; g-h) cellulose fibers after incubation for 20 days. Arrows with * show the disruption of the fiber cell wall.

The amorphous cellulose sample prepared by ball milling revealed no peak intensity from $2\theta = 10^\circ$ and $2\theta = 40^\circ$ and only a diffuse background (Fig. 4), typical of completely amorphous samples, as also reported by Agarwal *et al.* (2010) using 2 h of ball milling. Variances in crystal geometry can move (200) peak position, as observed for the pretreated fibers (Fig. 4). The peaks at $2\theta = 14.8^\circ$ and $2\theta = 16.3^\circ$ corresponds to the (1-10) and (110) lattice planes of cellulose I, respectively (Besbes *et al.*, 2011), and their overlapping can indicate a more amorphous sample, while its separation is related to an increase in crystallinity (Chan *et al.*, 2013). The separation of the peaks becomes more distinct for fiber exposed to enzymatic hydrolysis for 5 days, but less distinct for 10 and 20 days. This has been reported before, with higher separation for softwood hydrolyzed with cellulase and endoglucanase (Cao and Tan, 2004). The peak at around $2\theta = 35^\circ$ corresponding to (004) lattice planes became less sharp after hydrolysis as observed by Sathitsuksanoh *et al.* (2011). Similarly, the shoulder of the peak at around $2\theta = 20.5^\circ$ corresponding to the (012) and (102) planes has a tendency to increase in intensity by 10 and

20 days of enzymatic treatment, as reported by Cao & Tan (2005). However, French (2014) reported that (004) peak at around $2\theta = 35^\circ$ may be a composite of several reflections and change in its intensity, as well as the shoulder peaks, can indicate the absence of preferred orientation of the crystals. From these data, the crystallinity index (CI) and crystalline fraction (CF) were determined from Fig. 4 as described above in section 2 and are presented in Tab.2.

Fibers exposed to AD-supernatant exhibited a higher crystallinity index (CI) than the control due to the disruption of amorphous holocellulose (hemicelluloses + cellulose) surrounding and embedding the cellulose crystallites. As a consequence of the enzyme action (Hassan *et al.*, 2014) of the microorganisms from the AD-supernatant, it is important to emphasize that this apparent increase in crystallinity was most likely due to the removal of amorphous domains and not due to an increase in the order of less ordered regions. For CF, the variation in sample crystallinity is exclusively due to changes in cellulose crystalline structure, since the crystallographic information file (CIF) used in Mercury

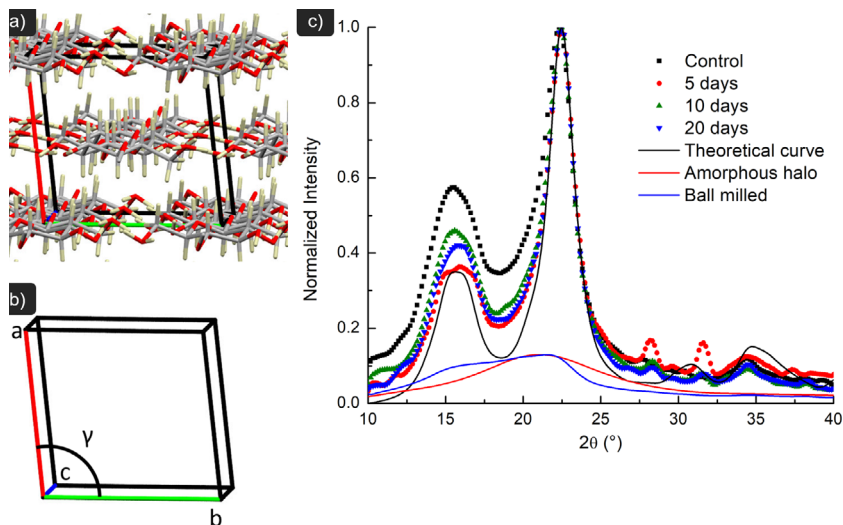


Fig. 4 a) Cellulose chains disposition in the unit cell; b) unit cell axes ('a', 'b' and 'c') and gamma angle used to modify patterns in Mercury software; c) X-ray diffraction (XRD) pattern of the milled fibers (control), fibers exposed to 5, 10 and 20 days in AD-supernatant, and amorphous cellulose obtained by ball milling treatment. The crystallinity index (CI) and crystalline fraction (CF) of amorphous cellulose was not determined because no diffraction peaks were detected or were too small to be measured.

Tab. 2 True density, crystallinity index (CI), crystalline fraction (CF), and crystallite size (CS) of the control (milled pulp) and fibers exposed to 5, 10 and 20 days in the liquid anaerobic digestate (AD-supernatant).

Cellulose condition	True density (g/cm ³)	CI (%)	CF (%)	CS (nm)
Control	1.44 ± 0.02	64	67	10
5 days	1.48 ± 0.03	75	68	11
10 days	1.61 ± 0.02	73	69	12
20 days	1.57 ± 0.05	72	68	12

program is just composed of cellulose instead of all the fiber components (cellulose + hemicellulose + lignin) to produce its theoretical diffraction patterns. This way, it is noted a clear tendency of increase in crystallinity with treated fibers, with higher crystallinity in 10 days exposure to the AD-supernatant. Even though Segal's crystallinity index has showed similar tendencies to crystalline fraction from Mercury, changes in the morphology of the peaks other than that related to plane (200) is not accounted for crystallinity in this method. It should be noted that Segal's crystallinity is a simplified method of crystallinity assessment providing no further information than an estimation of crystallinity (Nam *et al.*, 2016), being the theoretical analysis through Mercury software highly recommended by previous works (Correia *et al.*, 2016; Nam *et al.*, 2016; French *et al.*, 2014).

The decrease of CI with incubation periods greater than 5 days (i.e. 10 and 20 days) is due to the continuous degradation of both amorphous and crystalline domains with time. Another explanation for the lower crystallinity is that those samples may be composed of smaller crystals (French and Cintrón, 2013). During degradation, the intramolecular and intermolecular hydrogen bonding energy decreases (Lima *et al.*, 2014; Cao and Tan, 2004). It is expected that enzymes preferentially attack first the amorphous regions and then the small crystallites. Therefore, the crystallite size (CS) of the cellulose fibers increased during hydrolysis for the longer incubation periods (Tab. 2) as has also been previously reported (Cao and Tan, 2005). The accessibility of amorphous and crystalline regions of the cellulose structure is an important issue (Moxley *et al.*, 2008) since crystalline regions are degraded when amorphous regions are no longer accessible. As a result, crystal structures that were separated in the initial exposition to hydrolysis are readily accessible to degradation even when regions of less accessible amorphous material may still be existing. Table 2 also shows that true density of the cellulose fibers increases with the increase of CI and CF. This provides evidence that the amorphous regions (less packed structure in the fiber) were more readily and quickly hydrolyzed than the crystalline (more densified) regions.

Heat of dehydration and crystallinity determination by DSC

An endotherm peak in the range between 30 and 150°C was observed for all the samples (Fig. 5), which is assumed to be due to the dehydration (loss of adsorbed water). This endothermic peak occurs because of the energy required to balance the temperature difference between the hydrated sample and the reference in the DSC equipment. The amorphous cellulose sample obtained by ball milling

(and stored at 60% RH) presented the endothermic peak with a maximum latent heat of dehydration. The calculated latent heat of dehydration was around 199 ± 21 J/g, while the endothermic peak almost disappeared for the dried sample (Fig. 5). As reported elsewhere (Chan *et al.*, 2013; Bertran and Dale, 1986), this energy difference (latent heat of dehydration) is presumed to be because of vaporization of water adsorbed by the cellulose samples. It is assumed that water sorption in cellulose occurs first and almost totally in the amorphous sections, since cellulose crystals absorb only a small content of water. Therefore, a higher endothermic peak for water loss is expected for samples where the degree of crystallinity is lower.

The endothermic peak for fiber samples decreases as incubation periods in AD-supernatant increase from 5 days to 10 days (Fig. 5). The endothermic peak was larger when the crystallinity of the sample is lower. The mean values of latent heat of dehydration determined by DSC for all samples pre-conditioned at ambient temperature and 60% RH were compared with the corresponding calculated degree of crystallinity (DC) (Tab. 3). The data indicate that the latent heat of dehydration was positively correlated (with the exception of fiber exposed for 20 days) to the amorphous content of the samples (Tab. 3) and inversely correlated to the crystallinity index determined by XRD (Fig. 4 and Tab. 2). In the case of the fiber samples incubated for 20 days in AD-supernatant, the long-term exposure to degrading enzymes was assumed to increase the reducing end groups in the cellulose chains, increasing the OH groups available for water adsorption. This could explain the lower values of crystallinity determined by the DSC method compared to the XRD technique. In spite of these differences, the DSC method to determine crystallinity is useful as an alternative way to estimate the crystallinity of allomorphic forms of cellulose fibers, mainly for less crystalline samples (Bertran and Dale, 1986).

Thermogravimetry

The first degradation stage observed in the thermogravimetric analysis (TGA) occurred at the range of 150–350°C, with weight loss of around 60% for fibers incubated in AD-supernatant for 5 days and 10 days (Fig. 6a). The mass loss was 70% and 80% for the control and 20 days treatment, respectively. The onset degradation temperature (Tonset) of the fibers decreased with the incubation in AD-supernatant. The next thermal degradation stage occurred between 350 and 500°C. For temperatures higher than 500°C, no thermal event was observed.

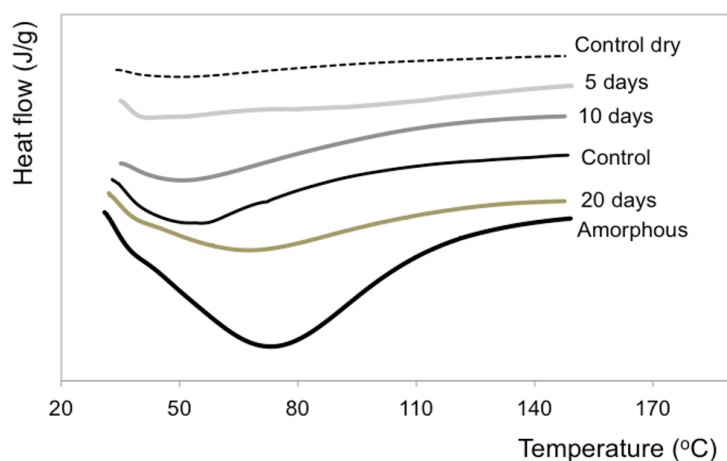


Fig. 5 DSC curves for milled fibers (control), fibers incubated for 5, 10 and 20 days in AD-supernatant, and amorphous cellulose obtained by ball milling treatment. With the exception of the control dry sample, all other samples were pre-conditioned at room temperature (~25°C) and around 60% RH in a desiccator containing KI and NH_4NO_3 saturated solutions.

Tab. 3 Heat of dehydration and degree of crystallinity (DC) determined by DSC for the cellulose fibers in the different conditions: amorphous cellulose obtained by ball milling; control (milled fiber) and fibers incubated for 5, 10 and 20 days in AD-supernatant. All samples analyzed here were previously conditioned at room temperature (~25°C) and 60% RH.

Cellulose condition	Heat of dehydration (J/g)	DC (%)
Amorphous (from ball milling)	199 ± 21	-
Control (milled pulp)	46 ± 8	77 ± 4
5 days	20 ± 4	90 ± 2
10 days	23 ± 5	88 ± 3
20 days	77 ± 11	61 ± 6

DTGA curves (Fig. 6b) also show that weight loss of the cellulose fibers happened in two stages. The thermogravimetric (DTGA) peak observed at around 330°C in the control sample corresponds to the weight loss of hemicelluloses (225-325°C), cellulose (305-375°C) and residual lignin (250-500°C) (Carrier *et al.*, 2011). Fibers treated with AD-supernatant thermally degraded at lower temperatures (Tonset around 260°C and maximum degradation at around 300°C). The enzymatic hydrolysis promoted by the presence of microorganisms in the treated samples caused this difference in thermal properties. Thermal stability of the cellulose molecule is reduced because the microorganisms generate exoglucanase-like enzymes that may cut the chains of cellobiose from the chain ends. Therefore, incubation in AD-supernatant increases the number of reducing end groups (REU) and decreases birefringence, hydrogen energy bonding, and DP of carbohydrate chains, decreasing the thermal stability of the fibers (Sharma and Varma, 2014).

As presented in Tab. 1, the AD-supernatant provided bacterial species that produced an extended range of enzymatic systems, most likely containing hydrolytic enzymes such as xylanases, that can degrade hemicelluloses present in the pulp fibers. Also, they may start the random hydrolysis of the β -1,4 non-reducing terminal regions located between the glycosidic linkages of glucose (Sathitsuksanoh *et al.*, 2011). The enzymatic hydrolysis of the amorphous regions of the fibrils needs to be controlled when the aim is to avoid degrading the crystalline domains

of cellulose fibrils. Decomposition of the solid residues in the control fibers occurred at around 450°C. Decomposition of the solid residues in the fibers exposed to AD-supernatant occurred at lower temperatures (425°C).

Finally, the whole concept of using a crude microbial preparation was to demonstrate that cellulose crystallinity could be changed without having to resort to specific enzyme treatments that are much more expensive. The anaerobic digestate used in this study is inexpensive and could be used to effectively aid in the pre-treatment of cellulose on large scale transformation processes, e.g. for making biofuels or for cellulose micro/nanofiber production.

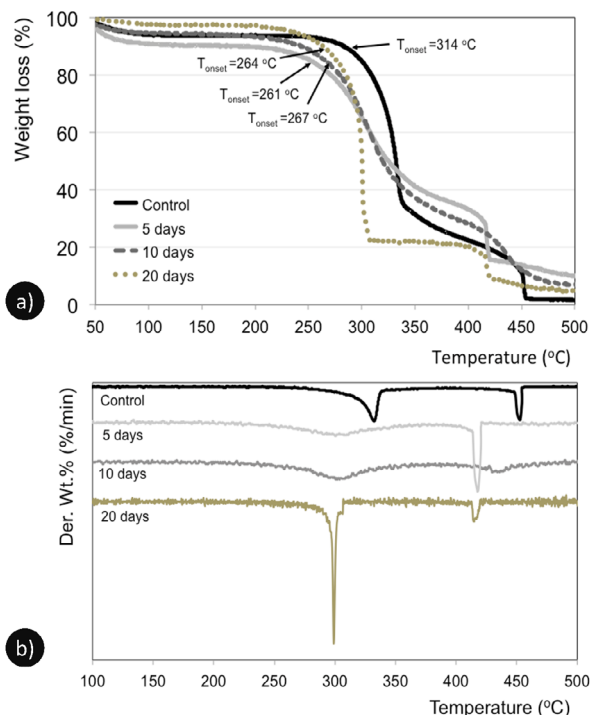


Fig. 6 (a) TGA thermograms (detail of the onset degradation temperature – Tonset); and (b) DTGA curves of the milled fibers (control), fibers incubated for 5, 10 and 20 days in AD-supernatant.

CONCLUSION

The bacterial species recognized in the AD-supernatant provided an extended range of extracellular enzymes for hydrolyzing lignocelluloses. The morphological and physical properties of eucalyptus pulp fiber were changed by incubating in AD-supernatant. Enzymatic hydrolysis partially removed the amorphous components of the pulp fiber resulting in a higher crystalline content. The increase in the crystallinity index (CI), crystalline fraction (CF) and crystallite size of cellulose was strong evidence that the amorphous portion of the cellulose was more readily and quickly hydrolyzed than the crystalline portion. The endotherm peak observed in the DSC measurement was assumed to be due to loss of adsorbed water, which was higher in the more amorphous samples. Therefore, higher water accessibility occurred when samples are less crystalline (exception for highly hydrolyzed samples – 20 days of exposition to AD-supernatant). This result mostly agrees with the results of XRD measurements. Enzymatic hydrolysis increased the number of reducing ends, leading to thermal degradation at lower temperatures. The increased incubation period resulted in substantial deconstruction of the cellulose structure as confirmed by the mass loss of the samples. Treatments with AD-supernatant may be useful for partially degrading pulp fiber for use in engineered fiber-based materials including production of high crystalline pulps, pulp bleaching and polymeric composites for a myriad of applications, and has a milder condition when compared to acid hydrolysis.

AUTHORSHIP CONTRIBUTION

Project Idea: GHDT,

Funding: GHDT, GG, WO

Database: GHDT, KH, DW, TW, AK

Processing: GHDT, KH, DW, TW, AK, GG, WO

Analysis: GHDT, KH, DW, LT, TW, ASF, AK

Writing: GHDT, KH, LT

Review: GHDT, JEO

REFERENCES

AGARWAL, U.P.; REINER, R.S.; RALPH, S.A. Cellulose I crystallinity determination using FT-Raman spectroscopy: univariate and multivariate methods. *Cellulose*, v. 17, p. 721–733, 2010.

BERTAN, M.S.; DALE, B.E. Determination of cellulose accessibility by differential scanning calorimetry. *Journal of Applied Polymers Science*, v. 32, p. 4241–4253, 1986.

BESBES, I.; VILAR, M.R.; BOUFI, S. Nanofibrillated cellulose from TEMPO oxidized eucalyptus fibres: Effect of the carboxyl content. *Carbohydrate Polymers*, v. 84, p. 975–983, 2011.

CAMPOS, A.; CORREA, A.C.; CANNELLA, D.; TEIXEIRA, E.M.; MARCONCINI, J.M.; DUFRESNE, A.; et al. Obtaining nanofibers from curauá and sugarcane bagasse fibers using enzymatic hydrolysis followed by sonication. *Cellulose*, v. 20, p. 1491–1500, 2013.

CAO, Y.; TAN, H. Structural characterization of cellulose with enzymatic treatment. *Journal of Molecular Structure*, v. 705, p. 189–193, 2004.

CAO, Y.; TAN, H. Study on crystal structures of enzyme-hydrolyzed cellulosic materials by X-ray diffraction. *Enzyme and Microbiology Technology*, v. 36, p. 314–317, 2005.

CARRIER, M.; LOPPINET-SERANI, A.; DENUX, D.; LASNIER, J.; HAM-PICHAVANT, F.; CANSELL, F.; et al. Thermogravimetric analysis as a new method to determine the lignocellulosic composition of biomass. *Biomass and Bioenergy*, v. 35, p. 298–307, 2011.

CHAN, C.H.; ZAKARIA, S.; AHMAD, I.; DUFRESNE, A. Production and characterization of cellulose and nano-crystalline cellulose from kenaf core wood. *Bioresources*, v. 8, p. 785–794, 2013.

CHASSARD, C.; DELMAS, E.; ROBERT, C.; BERNALIER-DONADILLE, A. The cellulose degrading microbial community of the human gut varies according to the presence or absence of methanogens. *FEMS Microbiology Ecology*, v. 74, p. 205–213, 2010.

CORREIA, V.C.; SANTOS, V.; SAIN, M.; SANTOS, S.F.; LEÃO, A.L.; SAVASTANO JUNIOR, H. Grinding process for the production of nanofibrillated cellulose based on unbleached and bleached bamboo organosolv pulp. *Cellulose*, v. 23, p. 2971–2987, 2016.

DURÃES, A. F. S.; MOULIN, J. C.; DIAS, M. C.; MENDONÇA, M. C.; DAMÁSIO, R. A. P.; THYGESEN, L. G.; et al. Influence of chemical pretreatments on plant fiber cell wall and their implications on the appearance of fiber dislocations. *Holzforschung*, v. 74, p. 949–955, 2020.

FONSECA, C. S.; SILVA, T. F.; SILVA, M. F.; OLIVEIRA, I. R. C.; MENDES, R. F.; HEIN, P. R. G.; et al. Eucalyptus cellulose micro/nanofibrils in extruded fibercomposite composites. *Cerne*, v. 22, p. 59–68, 2016.

FONSECA, A.S.; RAABE, J.; DIAS, L.M.; BALIZA, A. E. R.; COSTA, T. G.; SILVA, L. E. et al., Main Characteristics of Underexploited Amazonian Palm Fibers for Using as Potential Reinforcing Materials. *Waste and Biomass Valorization*, v. 10, p. 3125–3142, 2019.

FRENCH, A.D. Idealized powder diffraction patterns for cellulose polymorphs. *Cellulose*, v. 21, p. 885–896, 2014.

FRENCH, A. D. Increment in evolution of cellulose crystallinity analysis. *Cellulose*, v. 27, p. 5445–5448, 2020.

FRENCH, A.D.; CINTRÓN, M.S. Cellulose polymorphism, crystallite size, and the Segal Crystallinity Index. *Cellulose*, v. 20, p. 583–588, 2013.

HASSAN, L.M.; BRAS, J.; HASSAN, E.A.; SILARD, C.; MAURET, E. Enzyme-assisted isolation of microfibrillated cellulose from date palm fruit stalks. *Industrial Crops and Products*, v. 55, p. 102–108, 2014.

IMAI, M.; HORIKAWA, Y.; KIYOTO, S.; IMAI, T.; SUGIYAMA, J. Structural changes in sugarcane bagasse cellulose caused by enzymatic hydrolysis. *Journal of Wood Science*, v. 66, p. 1–8, 2020.

LE MOIGNE, N.; NAVARD, P. Dissolution mechanisms of wood cellulose fibres in NaOH-water. *Cellulose*, v. 17, p. 31–45, 2010.

LEJA, K.; CZACZYK, K.; MYSZKA, K. Biotechnological synthesis of 1,3-propanediol using *Clostridium* ssp. *African Journal of Biotechnology*, v. 10, p. 11093–11101, 2011.

LI, J.; ZHONG, H.; RAMAYO-CALDAS, Y.; TERRAPON, N.; LOMBARD, V.; POTOCKI-VERONESE, G.; et al. A catalog of microbial genes from the bovine rumen unveils a specialized and diverse biomass-degrading environment. *Gigascience*, v. 9, p. 1–40, 2020.

LIMA, J.T.; RIBEIRO, A.O.; NARCISO, C.R.P. Microfibril angle of *Eucalyptus grandis* wood in relation to the cambial age. *Maderas. Ciencia y Tecnología*, v. 16, p. 487–494, 2014.

MACRAE, C. F.; GRUNO, I. J.; CHISHOLM, J. A.; EDGINGTON, P. R.; MCCABE, P.; PIDCOCK, E.; et al. Mercury CSD 2.0-new features for the visualization and investigation of crystal structures. *Journal of Applied Crystallography*, v. 41, p. 466–470, 2008.

MEYABADI, T.F.; DADASHIAN, F. Optimization of enzymatic hydrolysis of waste cotton fibers for nanoparticles production using response surface methodology. *Fibers and Polymers*, v. 13, p. 313–321, 2012.

MOREIRA, L. R. S.; ÁLVARES, A. C. M.; SILVA, F. G.; FREITAS, S. M.; FERREIRA FILHO, E. X. Xylan-degrading enzymes from *Aspergillus terreus*: Physicochemical features and functional studies on hydrolysis of cellulose pulp. *Carbohydrate Polymers*, v. 134, p. 700–708, 2015.

MOXLEY, G.M.; ZHU, Z.; ZHANG, Y.H.P. Efficient sugar release by the cellulose solvent-based lignocellulose fractionation technology and enzymatic cellulose hydrolysis. *Journal of Agricultural and Food Chemistry*, v. 56, p. 7885–7890, 2008.

NAM, S.; FRENCH, A.D.; CONDON, B.D.; CONCHA, M. Segal crystallinity index revisited by simulation of X-ray diffraction patterns of cotton cellulose I β and cellulose II. *Carbohydrate Polymers*, v. 135, p. 1–9, 2016.

PRADO, N.R.T.; RAABE, J.; MIRMEHDI, S.; HUGEN, L.N.; LIMA, L.C.; RAMOS, A.L.S.; et al. Strength improvement of hydroxypropyl methylcellulose/ starch films using cellulose nanocrystals. *Cerne*, v. 23, p. 423–434, 2018.

- RABINOVICH, M.L.; MELNIK, M.S.; BOLOBOBA, A.V. Microbial cellulases (review). *Applied Biochemistry and Microbiology*, v. 38, p. 305-321, 2002.
- SATHITSUKSANO, N.; ZHU, Z.; WI, S.; ZHANG, Y.H.P. Cellulose solvent-based biomass pretreatment breaks highly ordered hydrogen bonds in cellulose fibers of switchgrass. *Biotechnology and Bioengineering*, v. 108, p. 521-529, 2011.
- SCAN STANDARD, C 1:77, Kappa number. Scandinavian Pulp, Paper and Board Testing Committee, 1977.
- SCAN STANDARD, C 4:61, Pentosans in pulp. Scandinavian Pulp, Paper and Board Testing Committee, 1961.
- SCAN STANDARD, C 6:62, Ash in wood and pulp. Scandinavian Pulp, Paper and Board Testing Committee, 1962.
- SCAN STANDARD, C 7:62, Dichloromethane extract of pulp. Scandinavian Pulp, Paper and Board Testing Committee, 1962.
- SEGAL, L.; CREELY, J.J.; MARTIN, A.E.; CONRAD, C.M. An empirical method for estimating the degree of crystallinity of native cellulose using the X-Ray diffractometer. *Textile Research Journal*, v. 29, p. 786-794, 1959.
- SHARMA, P.R.; VARMA, A.J. Thermal stability of cellulose and their nanoparticles: Effect of incremental increases in carboxyl and aldehyde groups. *Carbohydrate Polymers*, v. 114, p. 339-343, 2014.
- SILVA, E. L.; REIS, C. A.; VIEIRA, H. C.; SANTOS, J. X.; NISGOSKI, S.; SAUL, C. K.; et al. Evaluation of poly(vinyl alcohol) addition effect on nanofibrillated cellulose films characteristics. *Cerme*, v. 26, p.1-8, 2020.
- SILVA, L. E.; CLARO, P. I. C.; SANFELICE, R. C.; GUIMARÃES JÚNIOR, M.; OLIVEIRA, J. E.; UGUCIONI, J. C.; et al. Cellulose nanofibrils modification with polyaniline aiming at enhancing electrical properties for application in flexible electronics. *Cellulose Chemistry and Technology*, v. 53, p. 775-786, 2019.
- SIQUEIRA, G.; TAPIN-LINGUA, S.; BRAS, J.; PEREZ, D.D.; DUFRESNE, A. Morphological investigation of nanoparticles obtained from combined mechanical shearing, and enzymatic and acid hydrolysis of sisal fibers. *Cellulose*, v. 17, p. 1147-1158, 2010.
- SIRO, I.; PLACKETT, D. Microfibrillated cellulose and new nanocomposite materials: a review. *Cellulose*, v. 17, p. 459-494, 2010.
- TAN, H.Q.; LI, T.T.; ZHU, C.; ZHANG, X.Q.; WU, M.; ZHU, X.F. *Parabacteroides chartae* sp. nov., an obligately anaerobic species from wastewater of a paper mill. *International Journal of Systematic Evolutionary Microbiology*, v. 62, p. 2613-2617, 2012.
- TAPPI Useful Method, T 203cm-99: Alpha-, beta- and gamma-cellulose in pulp. TAPPI Standard Methods, 2009. 5p.
- TONOLI, G.H.D.; HOLTMAN, K.M.; GLENN, G.; FONSECA, A.S.; WOOD, D.; WILLIAMS, T., et al. Properties of cellulose micro/nanofibers obtained from eucalyptus pulp fiber treated with anaerobic digestate and high shear mixing. *Cellulose*, v. 23, p. 1-18, 2016.
- TONOLI, G. H. D.; TEIXEIRA, E. M.; CORREA, A. C.; MARCONCINI, J. M.; CAIXETA, L. A.; PEREIRA-DA-SILVA, M. A.; et al. Cellulose micro/nanofibers from Eucalyptus kraft pulp: preparation and properties. *Carbohydrate Polymers*, v. 89, p. 80-88, 2012.
- VIANA, L. C.; POTULSKI, D. C.; MUNIZ, G. I. B.; ANDRADE, A. S.; SILVA, E. L. Nanofibrillated cellulose as an additive for recycled paper. *Cerme*, v. 24, p. 140-148, 2018.
- WIRTH, R.; KOVÁCS, E.; MARÓTI, G.; BAGI, Z.; RÁKHELY, G.; KOVÁCS, K.L. Characterization of a biogas-producing microbial community by short-read next generation DNA sequencing. *Biotechnology and Biofuels*, v. 5, p. 1-16, 2012.
- WYMAN, C.E.; DECKER, S.R.; HIMMEL, M.E.; BRADY, J.W.; SKOPEC, C.E.; VIKARI, L. Hydrolysis of cellulose and hemicelluloses. In: S. DUMITRIU. *Polysaccharides: Structural diversity and functional versatility*. Marcel Dekker, Inc., 2004. p. 995-1033.
- YANG, B.; DAI, Z.; DING, S.Y.; WYMAN, C.E. Enzymatic hydrolysis of cellulosic biomass: a review. *Biofuels*, v. 2, 421-450, 2011.